Journal of Materials Chemistry B

RSC Publishing

PAPER

View Article Online
View Journal | View Issue

Cite this: *J. Mater. Chem. B*, 2013, **1**, 6129

Au coated Ni nanowires with tuneable dimensions for biomedical applications†

Kirsten M. Pondman,[a] A. Wouter Maijenburg,[b] F. Burcu Celikkol,[c] Ansar A. Pathan,[d] Uday Kishore,[d] Bennie ten Haken[a] and Johan E. ten Elshof*[b]

Received 6th June 2013
Accepted 13th September 2013

DOI: 10.1039/c3tb20808g

www.rsc.org/MaterialsB

Due to their shape anisotropy, high aspect ratio magnetic nanoparticles offer many advantages in biomedical applications. For biocompatibility, it is essential to have full control over the dimensions and surface chemistry of the particles. The aim of this study was to synthesize biocompatible nanowires with tuneable dimensions. This was achieved by electrodeposition of Ni in polycarbonate membranes. To ensure biocompatibility, a continuous gold coating was deposited onto the Ni wires by a newly developed electroless deposition method. The coating was analysed using electron microscopy and X-ray diffraction. Magnetic properties, anisotropy and Au film thickness were studied using vibrating sample magnetometry. After biofunctionalization, no significant cytotoxic effects were found in studies involving a diverse range of primary and tumour cells exposed to increasing concentrations of nanowires for up to 7 days. These nanowires may thus be used for *in vivo* applications such as magnetic drug delivery.

Introduction

Magnetic nanoparticles offer attractive possibilities in biomedicine, *e.g.* in magnetic separation, therapeutic drug, gene and radionuclide delivery, and hyperthermia, and as contrast agents in magnetic resonance imaging.[1] To date, the majority of magnetic nanoparticles used are spherical, consisting of one or multiple magnetic cores with a biocompatible coating and active ligands. Within biomedicine, magnetic nanowires are receiving growing attention.[2–6] Due to their elongated shape and anisotropic physical properties, these particles interact very differently with tissues, cells and biomolecules.[3,7–9] Due to their increased surface to volume ratio, more drugs and ligands can be bound for drug delivery or immunoassays. While the small diameter of nanowires makes it possible for the particles to pass through the narrow capillaries, the large remanent magnetization increases the range and effectiveness of magnetic interactions at a distance from external magnets. This allows not only magnetic drug targeting at locations deeper inside the body[4] and cell guidance,[10] but also increases the effectiveness of cell separation significantly.[6,9,11,12] Nanowires, with lengths matching the cell diameter, have previously been shown to outperform magnetic beads for cell separation, highlighting the importance of the dimensions of the nanowires.[9,11] Whereas spherical particles only respond to magnetic flux gradients, high aspect ratio particles allow the application of torque with a relatively weak external field to perform dynamic targeted cell therapy.[13] The torque can also be used to align the nanowires, and after their uptake by cells, it allows for the spatial organization of cells.[3,12]

Most research on elongated nanoparticles was performed with carbon nanotubes. This research showed that elongated particles are capable of entering cells by penetration, allowing for direct access to the cytosol without the need for endosome escape strategies.[7,14,15]

Several chemical methods to synthesize elongated nanoparticles can be found in the literature (Fig. 1).[16]

Templated electrodeposition has several advantages in this application, including ease of fabrication, reproducibility, and low cost. Nanowires made by this method are always

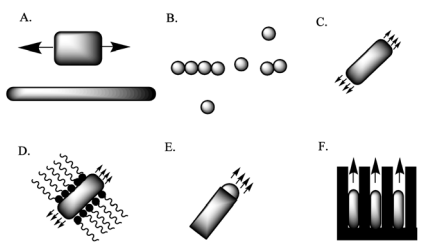

Fig. 1 (A) Size reduction of a 1D-microstructure; (B) (self)assembly of spherical nanostructures; (C) spontaneous synthesis by dictation by the anisotropic crystallographic structure of a solid; (D) kinetic control by a capping reagent; (E) confinement by a liquid droplet in a vapor–liquid–solid procedure; (F) direction through the use of a template.

[a]*Neuro Imaging, MIRA Institute, University of Twente, Enschede, The Netherlands*
[b]*Inorganic Material Science, MESA+ Institute for nanotechnology, University of Twente, Enschede, The Netherlands. E-mail: j.e.tenelshof@utwente.nl*
[c]*Nanobiophysics, MIRA Institute, University of Twente, Enschede, The Netherlands*
[d]*Centre for Infection, Immunity and Disease Mechanisms, Biosciences, Brunel University, London, UK*

† Electronic supplementary information (ESI) available: Control cell microscopy images of RAW 264.7 and Jurkat cells. See DOI: 10.1039/c3tb20808g

continuous since any breakage would halt the growth of the nanowires. Depending on the template and deposition time used, nanowires can be made with nanometer to micrometer dimensions, spanning several relevant biological length scales. Various magnetic metals such as iron (Fe), cobalt (Co) and nickel (Ni), and their alloys have been used to form nanowires inside the pores of silica, anodized alumina, or polycarbonate membranes.[17–20]

Having full control over the dimensions of nanowires is essential for biomedical applications. Previous research on asbestos and carbon nanotubes has suggested that cytotoxicity is highly dependent on aspect ratio. Long nanowires have been associated with inflammation, fibrosis and malignant mesothelioma and are likely to generate reactive oxygen species that can cause DNA damage and cell death.[21] Unfortunately, most proposed nanowires[8,9,22] are larger than cells, leaving the wires to protrude from the cells, thereby reducing the viability of the cells. Particles longer than 5 μm cannot be considered as "safe" in terms of uptake and clearance by macrophages and possibly induce inflammation and carcinogenic effects.[23] A length below 5 μm will also make it possible for the nanowires to flow through the curvy capillaries allowing for local drug delivery.

In addition to dimensional restrictions, the materials and surface chemistry of the particles should be biocompatible and stable during use. Fe is often considered the most advantageous option, but due to the ease of oxidation of Fe, Ni is often preferred as a magnetic phase for nanowires. Although Ni is a naturally occurring transition material and an essential nutrient,[24] there are indications that Ni may be a carcinogen and induce apoptosis.[25–27] Studies on the toxicity of Ni wires are divided; some studies indicate no toxicity of Ni nanowires at low concentrations, and the need for long term exposure to act as carcinogens.[4,28] But at higher concentration, even short incubation times have been shown to be lethal to cells.[8] Some authors indicate the benefits of induced apoptosis by Ni nanowires, *e.g.* reactive oxygen species mediated apoptosis caused by Ni nanowires in human pancreatic adenocarcinoma cells.[29] Unfortunately, these apoptotic effects are not specific to carcinoma cells and would therefore also occur in other healthy bystander cells. Shielding of the potentially toxic Ni from contact with the body was therefore considered essential in this study. The coating is also important to protect the Ni from oxidation. For this purpose, various polymers, proteins and phospholipids have been proposed.[22,30,31] These coatings are biocompatible but cannot shield the particles from oxygen. Therefore, a solid Au shell is considered most advantageous as Au is known for its excellent biocompatibility and it cannot be removed by factors within the body.[32] Furthermore, Au provides a platform for functionalization, such as conjugation of biomolecules, and targeting moieties and drugs.[33,34]

This work aims at the development of a magnetic nanowire for application in magnetic drug delivery and similar biomedical applications. The proposed electrodeposited Ni nanowire has a tuneable length below 5 μm with narrow size distribution. To increase the biocompatibility, the nanowires were coated with an Au shell. To limit toxic effects, the use of cyanide, which is commonly used in Au coatings,[32] was avoided. Therefore, a new coating procedure was developed, inspired by a method to synthesize Au nanotubes by electroless deposition.[35] The nanowires were characterized using a variety of techniques in order to determine their dimensions, magnetic properties, crystallographic structure and biocompatibility.

Materials and methods

Materials

Commercially available polycarbonate track-etched membranes (PCTE, Whatman, UK) with a nominal (quoted by the supplier) pore size of 50 nm were used as template membranes. Nickel(II) sulfate hexahydrate ($NiSO_4 \cdot 6H_2O$), boric acid (H_3BO_3), ammonia (NH_4OH, 37%), and glutathione (GSH) were obtained from Sigma-Aldrich and were used without further purification. Thiolated polyethylene glycol (mPEG-SH, 2 kDa) was purchased from Rapp Polymere (Tübingen, Germany). Dichloromethane (CH_2Cl_2) was used as obtained from Thermo Fisher Scientific (Waltham, USA). Trifluoroacetic acid, 11-aminoundecanoic acid, sodium sulfite (Na_2SO_3), sodium carbonate ($NaHCO_3$), silver nitrate ($AgNO_3$), and formaldehyde were purchased from Acros (Geel, Belgium). Tin(II) chloride ($SnCl_2$) was purchased from Alfa Aesar (Ward Hill, USA). Oromerse-B was purchased from Technic Inc. (Cranston, RI, USA). Materials for cell culture: Dulbecco's modified Eagle medium (DMEM) and fetal bovine serum (heat inactivated) were purchased from PAA laboratories (Pasching, Austria), penicillin–streptomycin, trypan blue and phosphate buffered saline (PBS) from Invitrogen (Carlsbad, CA, USA), and CellTiter-Blue (CTB) from Promega Corp (Madison, WI).

Nanowire synthesis

Ni nanowires were synthesized by templated electrodeposition in a conventional three-electrode setup. First, an Au layer was sputtered onto a PCTE membrane with a pore size of 50 nm using a Perkin-Elmer 2400 sputtering system under Ar. The Au layer (also called the back electrode) was used as the working electrode in the electrochemical deposition process. Prior to deposition, the backside of the back electrode was isolated using a glass plate. A small Pt mesh was used as the counter electrode and Ag/AgCl in 3 M KCl (Metrohm Autolab) was used as the reference electrode. All reported potentials are with respect to the reference electrode. The electrodes were connected to a potentiostat (Autolab PGSTAT 128N from Metrohm Autolab, Netherlands). For electrodeposition of nanowires, the electrodes were placed inside a plating solution containing $NiSO_4 \cdot 6H_2O$ (1.4 M) and H_3BO_3 (0.73 M), and a voltage of −1.0 V *versus* reference was applied for 6 min.

After deposition, the membranes were dissolved in dichloromethane and washed at least 3 times with dichloromethane and 3 times with MilliQ water by centrifugation.

Electroless Au coating of Ni nanowires

Au coating was achieved using 5 subsequent steps adapted from ref. 31 as depicted schematically in Fig. 2.

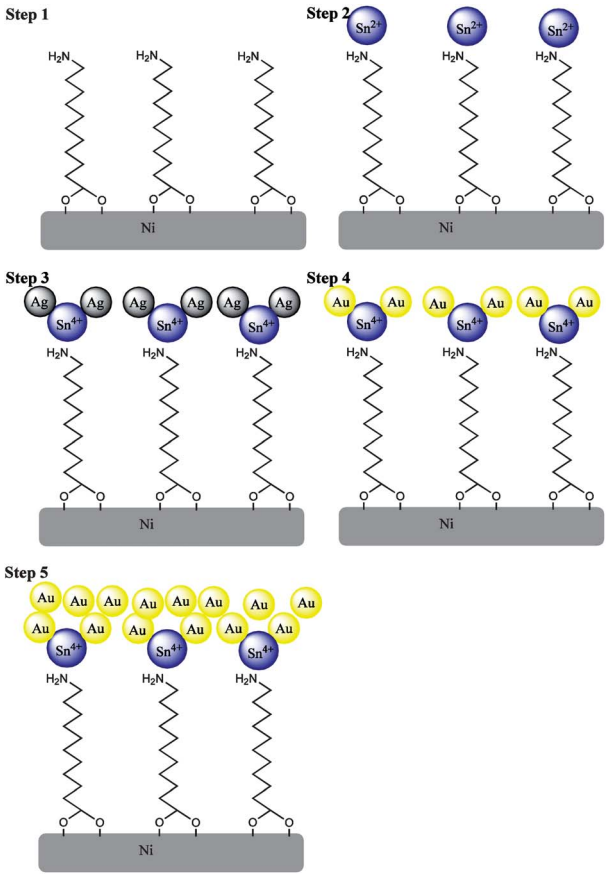

Fig. 2 Scheme showing stepwise Au coating on Ni nanowires. (1) Amination, (2) Sn^{2+} deposition, (3) Ag deposition, (4) replacement of Ag by Au and (5) growth of the Au layer.

Clean Ni nanowires were dispersed by sonication in an aqueous solution of 10 mM 11-aminoundecanoic acid for 2 h, to form an aminated monolayer (step 1 in Fig. 2). The nanowires were then washed at least 3 times with H_2O.

A fresh aqueous solution containing 54 mM $SnCl_2$ and 70 mM trifluoroacetic acid was added to the nanowires for 45 min. Sn(II) ions interacted with the electronegative amine groups forming a layer of electrostatically bound Sn^{2+} on the surface (step 2 in Fig. 2). After incubation, the nanowires were washed repeatedly with H_2O.

Sn^{2+} was oxidized by Ag^+ *via* $Sn^{2+} + 2Ag^+ \rightarrow Sn^{4+} + 2Ag^0$, by adding an aqueous solution containing 29 mM $AgNO_3$ and 100 mM NH_4OH (step 3 in Fig. 2). After repeated washing with H_2O, the Ag phase can be replaced by Au.

A solution of 1 g Na_2SO_3, 0.6 g $NaHCO_3$, 6 mL $Na_3Au(SO_3)_2$ (Oromerse B) and 480 mL H_2O was prepared. The nanowires were placed in 10 mL aliquots of this solution and sonicated at 3.6 °C for 30 min.

To allow for the formation of a closed layer of Au on the Ni nanowires, 25 μL mL^{-1} formaldehyde was added to the solution. This destabilized the Au^+–sulfite complex, and induced the galvanic replacement reaction $Ag^0 + Au^+ \rightarrow Ag^+ + Au^0$ (steps 4 and 5 in Fig. 2), and further electroless growth of the Au layer. The nanowires were sonicated for 12 h at 3.6 °C, and washed at least 5 times with H_2O to remove free ions. Nanowires prepared using this method are named Au–Ni nanowires.

Biofunctionalization

The biofunctionalization of the Au–Ni nanowires was accomplished by incubating 100 μg mL^{-1} Ni or Au–Ni nanowires with 9 mM glutathione and 1 mM mPEG-SH in PBS for 24 h at 4 °C. Excess surfactant was removed by washing with PBS. The functionalization was analysed by Fourier transform infrared spectroscopy (FTIR, Thermo Scientific smart orbit Nicolet 6700 ATR-IR spectrometer) on KBr pellets with 0.5% dried and crushed Au–Ni nanowires.

Characterization

Analysis of the nanowires was performed with a Zeiss HR-LEO 1550 FEG Scanning Electron Microscope (SEM) operating at 2.0 kV. X-ray diffraction (XRD) was performed on samples randomly deposited on a glass plate with a Bruker D2 Phaser with a Cu Kα X-ray source and a wavelength of 1.54 Å.

Magnetic characterization was performed using a vibrating sample magnetometer (Model 10 Mark II VSM, Microsense). Samples were dried in a glass container before measurement; a blank measurement was subtracted from the sample data. Dispersed samples were measured in a glass container closed with Parafilm, and a blank containing the liquid in which the dispersion was made was subtracted from the data.

Cell culture

A number of tumour as well as non-tumour cell lines were used to assess the effect of nanoparticles on cell viability. These included: THP1 (a monocytic cell line derived from acute monocytic leukemia); Jurkat cell line (a T cell line derived from acute T cell leukemia); U937 (a monocytic cell line derived from histiocytic lymphoma); Raji (a B cell line derived from Burkitt's lymphoma); GBM (a primary cell line derived from glioblastoma multiforme); HeLa (a human cervical carcinoma epithelial cell line); A431 (an epithelial cell line derived from epidermoid carcinoma); RAW 264.7 (a murine macrophage cell line) and A549 (an epithelial cell line derived from lung carcinoma). The non-adherent cell lines THP1, Jurkat, U937, and Raji cell lines were grown in complete RPMI containing 10% heat inactivated FCS, 2 mM L-glutamine, 100 U mL^{-1} of penicillin and 100 μg mL^{-1} of streptomycin and 1 mM of sodium pyruvate, whereas adherent cell lines A431, A549 and GBM, and RAW 264.7 and HeLa were grown in complete DMEM containing the above mentioned supplements.

Human monocytes and lymphocytes, and PBMC were isolated from blood samples from 2 healthy subjects using Ficoll-Paque plus (GE Healthcare) gradient according to the manufacturer's instructions. PBMC obtained from the interface of plasma and Ficoll-Paque were washed twice with RPMI and suspended in complete RPMI. 5×10^6 PBMC in complete RPMI were plated out in each well of a 6 well plate (SPL Life Sciences), and pre-coated with human AB serum overnight. After 2 h of incubation at 37 °C in 5% CO_2, the non-adherent PBMC (containing T, B and NK cells) were gently removed from adherent cells (monocytes).

Confocal imaging

A Zeiss (Göttingen, Germany) LSM 510 confocal laser scanning microscope (CLSM) was used to image uptake of Au–Ni nanowires by cells in bright field. 10^4 cells per well were incubated in a 96-well plate. Cells were allowed to adhere for 2 h after which Au–Ni nanowires were added with a nanowire concentration of approximately 10 nanowires per cell. This concentration was estimated by assuming that the nanowires have the density of bulk Ni and Au and average dimensions as estimated from SEM images. Control samples contained no nanowires. Images were obtained after 24 h incubation at 37 °C in a 5% CO_2 atmosphere.

Concentration dependent short term cell viability on phagocytotic and non-phagocytotic cells

Adherent cells, RAW 264.7 and HeLa, were seeded on 96-well culture plates at 5×10^3 cells per well in 100 μL of cell medium. Cells were allowed to adhere to the plate for 24 h at 37 °C in a 5% CO_2 atmosphere. Incubation of Ni and Au–Ni nanowires was done by adding 100 μL of Au–Ni nanowire dispersion in cell medium to the cells on the 96-well culture plates, for 48 h at 37 °C in a 5% CO_2 atmosphere. The final concentrations of the Au–Ni nanowires were 0, 1, 10, 100 and 1000 nanowires per cell. All experiments were performed in triplicate.

After 48 h the cell medium was carefully removed and the cells were washed with PBS, thereafter 100 μL of cell medium was added with 10 μL of CellTiter-Blue and incubated for 4 h. The fluorescence was measured on a spectrophotometer (Victor, Perkin Elmer) with an excitation wavelength of 560 nm and an emission wavelength of 590 nm. The fluorescence values were normalized by the controls and expressed as percent viability. Validity of the assay was assessed by cell counting and visual inspection of the cells.

Long term cell viability following exposure to Au–Ni nanowires

The long term cytotoxicity of Au–Ni nanowires was investigated by measuring viable and dead cells. Non-adherent cells were seeded at 10^5 cells per well and adherent cells at 2×10^4 cells per well and were allowed to adhere for 2 h at 37 °C in 5% CO_2. Au–Ni nanowires in PBS were added to duplicate wells at a concentration of 100 nanowires per cell. Duplicate control wells were treated with an equal volume of PBS. The cells were then incubated at 37 °C in 5% CO_2 for 12 h, 1, 2, 5 and 7 days. At each time point, the cells were suspended (using trypsin–EDTA to detach adherent cells). 20 μL of the cell suspensions were then mixed with an equal volume of trypan blue (0.4%). At least 100 cells from each duplicate culture were observed for the morphology and staining of cells using a haemocytometer and an inverted microscope (Leica). Blue stained cells were considered dead. Adherent and non-adherent PBMC were cultured at 5×10^5 cells per well and the ratio of cells to nanowires was similar to other cell lines. Approximately 200 cells from each culture were observed under the microscope using trypan blue at each time point as mentioned above.

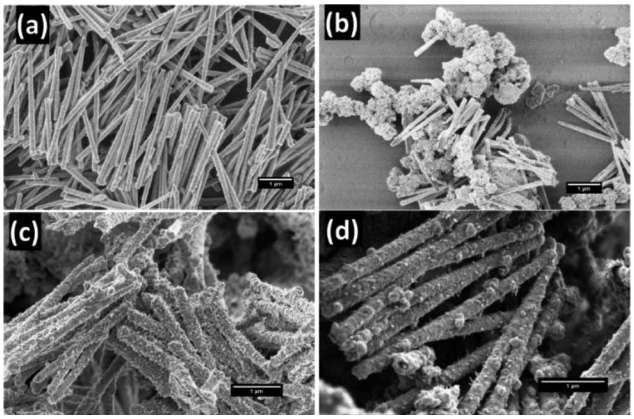

Fig. 3 HR-SEM images of Ni nanowires and Au–Ni nanowires. (a) Original Ni nanowires, (b) Oromerse-B Ni nanowires, (c) Sn–Ag–Au–Ni nanowires, and (d) 11-aminoundecanoic acid–Sn–Ag–Au nanowires, hereafter indicated as Au–Ni nanowires.

Results and discussion

Ni nanowires with an average diameter of 150 nm and a length of 2.6 ± 0.3 μm (SEM, $n = 100$) were obtained by electrodeposition of Ni in the pores of a PCTE membrane for 6 min at −1.0 V *versus* an Ag/AgCl reference electrode. The nanowires were released into suspension by dissolving the membrane and several washing steps with dichloromethane and water. An Au coating was deposited by electroless deposition onto the Ni nanowires and the morphology of the Au-coated Ni nanowires was investigated by HR-SEM as shown in Fig. 3.

Employing only the Au deposition reaction with Oromerse B (steps 4 and 5 in Fig. 2) did not result in Au nucleation on the Ni nanowire surface as can be seen in Fig. 3b. Therefore, an activation step was introduced in which Sn nuclei were deposited, followed by galvanic replacement by Ag, and finally growth of Au on the Ag nuclei. Unfortunately, the Au coating was still discontinuous (Fig. 3c), most likely due to an insufficient concentration of Sn nuclei on the Ni surface. An amination step, using 11-aminoundecanoic acid, was introduced to provide more homogeneous Sn deposition, allowing a continuous Au coating to form over the entire nanowire surface (Fig. 3d), with an approximate

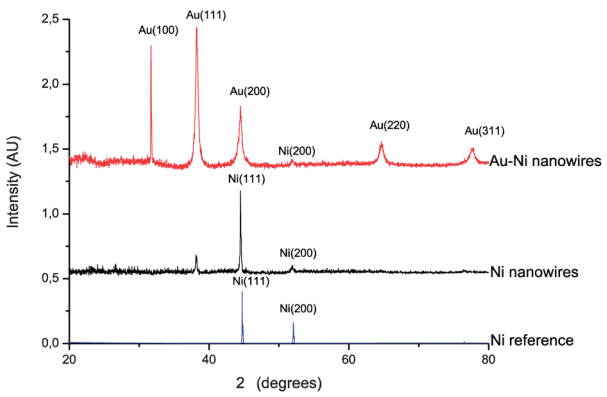

Fig. 4 XRD patterns of randomly oriented Ni nanowires and Au–Ni nanowires and a pure Ni reference sample.

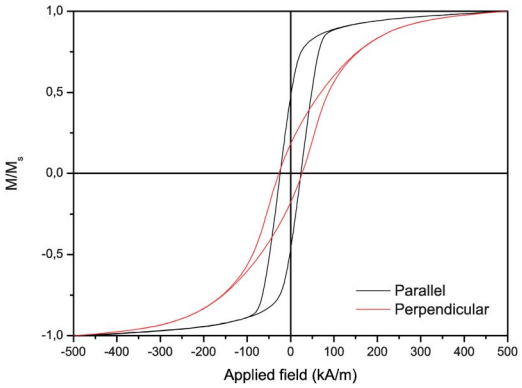

Fig. 5 Magnetic hysteresis curves of Ni nanowires measured inside the membrane under an external field parallel and perpendicular to the nanowire long axis. Parallel coercivity value of 302 Oe and $M_r/M_s = 0.48$ and perpendicular coercivity of 378 Oe and $M_r/M_s = 0.17$.

thickness of 40 nm as estimated from SEM. Longer Au deposition will result in the formation of a thicker Au layer.

The phase and grain size of the Ni nanowires and Au coating were investigated by XRD (Fig. 4). Ni nanowires showed diffraction peaks corresponding to the (111) and (200) planes of cubic Ni. The peak at 2θ 38° can be assigned to the Au (111) plane of the back electrode. After the complete Au coating procedure diffraction peaks were detected, which can be assigned to Au (110), (111), (200), (220) and (311). The Ni (111) and Au (200) peaks overlap, therefore it is not possible to distinguish between them. The broader peaks in the Au spectrum compared to the Ni spectrum indicate a smaller crystallite size for the Au layer. Using the Debye–Scherrer equation $\tau = K\lambda/\beta \cos\theta$, the crystallite sizes of Ni and Au can be estimated. Here, τ is the mean size of the crystalline domain, K the shape factor, β the full width at half maximum, θ the Bragg angle and λ the X-ray wavelength. The estimated crystallite sizes are 54 nm for Ni and 20 nm for Au. By comparing the crystallite sizes from XRD with SEM imaging, we can conclude that the crystalline domain size in the central Ni nanowire is about 1/3 of its diameter, and it is surrounded by an Au layer with an equivalent thickness of about 2 grains.

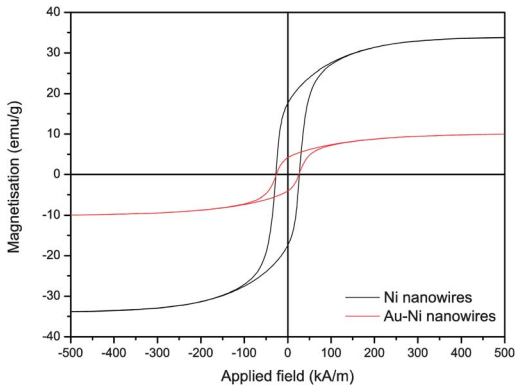

Fig. 6 Hysteresis curves of Ni nanowires and Au–Ni nanowires in random orientation under an external field. $M_s = 34$ emu g^{-1} for uncoated and $M_s = 10$ emu g^{-1} for Au coated Ni nanowires, suggesting a coating thickness of 34 nm on a 2.6 μm long Ni nanowire with 150 nm diameter.

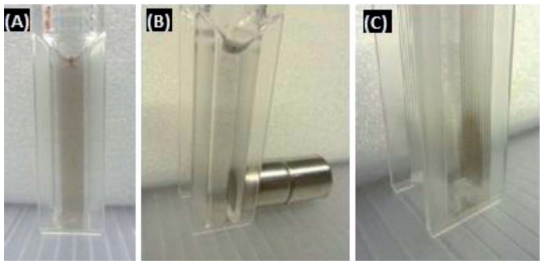

Fig. 7 (a) Suspension of Au–Ni nanowires stabilised with GSH and mPEG-SH. (b and c) The Au–Ni nanowires can be collected using a permanent magnet.

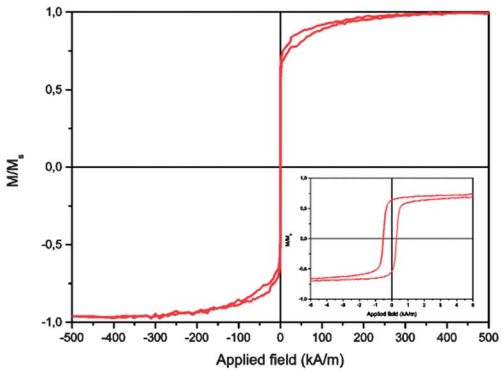

Fig. 8 Magnetisation loop M *vs.* applied field H for suspended Au–Ni nanowires showing superparamagnetic behaviour. The inset shows that the coercivity of the Au–Ni nanowires is approximately 1 kA m^{-1} for dispersed samples.

Fig. 5 shows the room temperature magnetization curves for uncoated Ni nanowires inside the template with magnetic field (H) applied in two directions, *i.e.* parallel and perpendicular to the wire direction. The squareness ratio M_r/M_s and coercivity are known to increase significantly with aspect ratio.[36] The obtained hysteresis loops show magnetic anisotropy where the magnetic easy direction is along the axis, as can be seen from the squareness ratio $M_r/M_s = 0.48$ in the parallel direction. From VSM measurements on randomly orientated nanowires as depicted in Fig. 8 the saturation magnetization of the Ni nanowires was found to be 34 emu g^{-1}, which is significantly

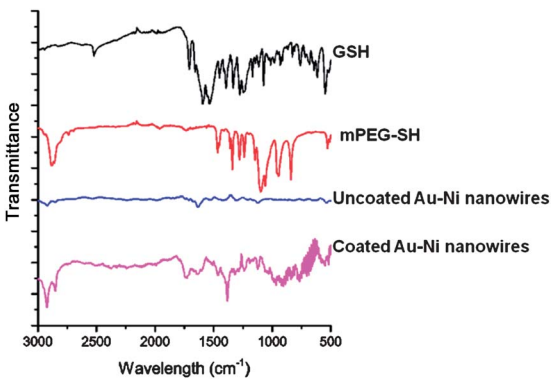

Fig. 9 FTIR spectra of GSH, mPEG-SH, and uncoated Au–Ni nanowires, and the attachment of GSH and mPEG-SH to the Au–Ni nanowires.

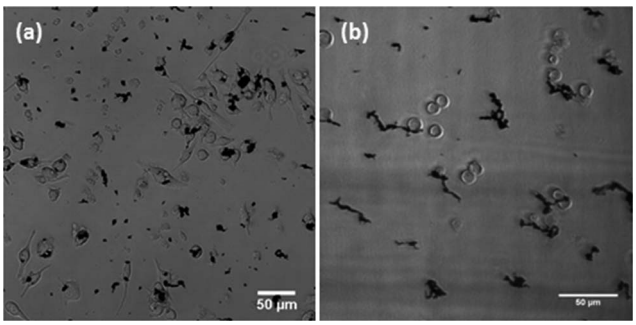

Fig. 10 Interaction of Au–Ni nanowires with (a) RAW 264.7 cells and (b) Jurkat cells.

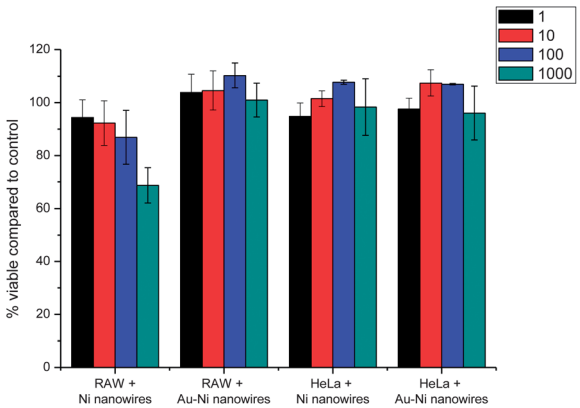

Fig. 11 Short term viability compared to untreated control of RAW and HeLa cells assessed by CTB assay after 48 h incubation with Ni and Au–Ni nanowires. The bars indicate standard deviation.

less than the value for bulk Ni (55.4 emu g^{-1}). This can be explained by the surface anisotropy which is significant for a wire with small diameter. After Au coating of the Ni nanowires the saturation magnetization decreased to 10 emu g^{-1} (Fig. 6). From this value, the diameter and length of the Ni nanowire and the densities of Ni (8.9×10^6 g m^{-3}) and Au (19.3×10^6 g m^{-3}), the shell thickness can be calculated. Neglecting the influence of the other coating layers the Au layer thickness is approximately 34 nm, which is in good agreement with the thickness estimated from HR-SEM images.

After biofunctionalisation using SH-PEG and glutathione, a suspension of Au–Ni nanowires was obtained (Fig. 7). The nanowires could be easily collected using a permanent magnet and dispersed by vortexing. Due to the possibility to move freely in the liquid, the magnetization curves of suspended nanowires showed superparamagnetic behaviour, with no remnant magnetisation (Fig. 8). Attachment of GSH and mPEG-SH was examined by FTIR spectroscopy (Fig. 9). GSH attachment can be identified by two bands around 1600 cm^{-1} for both cysteine and glutamic acid-carbonyl. The anchoring is *via* the thiol group as the band at 2500 cm^{-1} for SH stretching is not visible on the Au–Ni nanowires. Binding of mPEG-SH can be seen by a strong band at 1380 cm^{-1} showing C–H stretching, and the band at 1080 cm^{-1} shows C–O–C stretching from mPEG-SH.

The uptake of Au–Ni nanowires was studied by confocal microscopy (Fig. 10). 3D imaging (not shown here) ascertained that the particles were inside the cells and not simply adhered to the membrane. After 24 h of incubation, RAW 264.7 cells had taken up many nanowires and clusters of nanowires. As these cells are macrophages, the uptake pathway is most likely phagocytosis. Confocal microscopy analysis showed that the nanowires were completely taken up by these cells without signs of frustrated phagocytosis. This indicates that macrophages will be able to remove the particles from the bloodstream. Jurkat cells are not capable of phagocytosis and only take up particles by receptor mediated endocytosis. As expected, these cells did not take up any nanowires, and appeared as healthy as control untreated cells (see ESI†).

The effects of Au–Ni nanowires on cell viability were evaluated using a CTB assay. Au–Ni nanowires did not show a decrease in cell viability of both HeLa and RAW cells over 48 h (Fig. 11). In a study between phagocytic and non-phagocytic cells, a slightly higher cytotoxicity was observed for phagocytic

Table 1 Long term viability of 9 different cell lines showed no significant cytotoxicity

Cell type		12 h	24 h	48 h	5 days	7 days
U937 (non-adherent)	Control	97.6 ± 1.0	96.3 ± 0.6	96.9 ± 0.4	98.1 ± 0.4	97.2 ± 0.1
	Au–Ni wires	96.5 ± 0.7	96.5 ± 0.7	96.7 ± 0.6	98.7 ± 1.4	98.2 ± 1.2
THP1 (non-adherent)	Control	99.7 ± 0.5	95.7 ± 0.1	98.0 ± 1.5	99.0 ± 0.3	98.5 ± 0.4
	Au–Ni wires	98.5 ± 0.5	93.7 ± 0.1	95.5 ± 1.8	99.0 ± 0.4	99.3 ± 0.3
A549 (adherent)	Control	95.3 ± 1.4	98.1 ± 0.6	92.9 ± 0.3	98.5 ± 1.4	97.0 ± 0.9
	Au–Ni wires	98.8 ± 0.6	98.6 ± 0.2	94.2 ± 1.4	98.5 ± 1.3	96.6 ± 0.7
Raji (non-adherent)	Control	97.7 ± 0.3	98.2 ± 0.4	98.7 ± 0.1	99.5 ± 0.1	96.6 ± 0.6
	Au–Ni wires	97.9 ± 0.1	97.7 ± 0.4	98.6 ± 0.7	98.4 ± 0.4	95.4 ± 2.9
GBM (adherent)	Control	98.7 ± 0.1	97.8 ± 3.1	99.1 ± 0.5	96.0 ± 0.7	96.3 ± 2.5
	Au–Ni wires	98.9 ± 0.2	98.4 ± 0.0	98.7 ± 0.7	96.1 ± 0.7	97.1 ± 0.9
Jurkat (non-adherent)	Control	98.4 ± 0.3	96.9 ± 0.6	97.8 ± 0.7	94.6 ± 0.8	93.6 ± 1.7
	Au–Ni wires	97.8 ± 0.5	97.9 ± 0.2	98.1 ± 1.0	94.6 ± 0.1	92.0 ± 1.0
PBMC (adherent)	Control	99.5 ± 0.2	98.4 ± 0.6	99.5 ± 0.4	98.4 ± 1.0	98.4 ± 0.5
	Au–Ni wires	99.8 ± 0.2	99.3 ± 0.5	99.5 ± 0.4	98.4 ± 0.9	98.5 ± 0.4
PBMC (non-adherent)	Control	99.5 ± 0.4	97.8 ± 0.9	99.8 ± 0.3	96.3 ± 1.3	98.2 ± 0.9
	Au–Ni wires	99.6 ± 0.4	98.5 ± 0.8	99.7 ± 0.2	96.1 ± 1.4	97.7 ± 0.6
A431 (adherent)	Control	98.7 ± 0.1	98.6 ± 0.1	96.2 ± 1.9	96.1 ± 3.8	96.1 ± 3.8
	Au–Ni wires	98.9 ± 0.2	98.2 ± 1.1	95.6 ± 0.2	95.2 ± 1.7	95.2 ± 1.7

(RAW 264.7) cells compared to non-phagocytic (HeLa) cells, which might indicate the importance of uptake on cytotoxicity. It should be noted that the high concentration of 1000 nanowires per cell is much higher than targeted in potential applications in biomedicine, and is only used here to investigate the biocompatibility of the nanowires. In RAW cells Ni nanowires showed increased cytotoxicity compared to the Au coated Ni nanowires, indicating the necessity of the Au coating. The used concentration of nanowires is much higher than the lethal concentration of Ni nanowires with a length of 20 μm found by Byrne *et al.*,[8] which indicates and illustrates the high biocompatibility of the much shorter Ni and Au–Ni nanowires.

A range of cells – primary and cancerous, phagocytic and non-phagocytic, adherent and non-adherent – were used in order to systematically investigate cytotoxicity over a long term (Table 1). All 9 different cell types used in this study did not show significant cytotoxicity of the Au–Ni nanowires for periods up to 7 days.

Conclusions

Biocompatible nanowires with tuneable dimensions were prepared by templated electrodeposition of Ni in PCTE membranes. The dimensions of the nanowires can be fully tuned by adapting the deposition time and template dimensions. An Au coating procedure was developed to ensure biocompatibility by complete shielding of the Ni phase from the biological environment. The newly developed procedure involves amination of the Ni surface, activation by Sn and Ag, followed by electroless Au deposition. A coating thickness of approximately 40 nm was achieved by 12 h electroless Au deposition. SEM imaging shows a smooth and continuous layer of Au on the Ni nanowires. Elemental analysis confirmed the formation of Au on Ni. Magnetic measurements were used to reveal the shape anisotropy and ferromagnetic properties of the Au–Ni nanowires. Stable suspensions of nanowires were obtained by biofunctionalisation using GSH and mPEG-SH. Cell studies indicate that the nanowires can be completely engulfed by cells without signs of frustrated phagocytosis. No significant cytotoxic effects and morphological alterations were found when nanowires were exposed to a variety of cell lines, indicating the potential use of the nanowires in biomedical applications, such as magnetic drug delivery.

Conflict of interest

The authors declare no competing financial interest.

Acknowledgements

Financial support from the Chemical Sciences division of the Netherlands Organization for Scientific Research (NWO-CW) is gratefully acknowledged. The authors thank R. Besselink (Inorganic Materials Science) for support and suggestions, M. Sobik (Neuro Imaging) for data acquisition and interpretation and M.M.S.M. Wösten (University Utrecht, Veterinary Faculty Division infection biology) and Robert Sim (Oxford University, Department of Pharmacology) for advice on cell viability tests.

References

1 Q. A. Pankhurst, J. Connolly, S. K. Jones and J. Dobson, *J. Phys. D: Appl. Phys.*, 2003, **36**, R167–R181.
2 Q. Hu, Y. Q. Liu, N. Li, C. Cheng, S. G. Xu, N. Wang, W. Qin and B. Z. Tang, *Nano*, 2013, **8**, 1350029.
3 A. Hultgren, M. Tanase, C. S. Chen, G. J. Meyer and D. H. Reich, *J. Appl. Phys.*, 2003, **93**, 7554–7556.
4 A. Prina-Mello, Z. Diao and J. M. Coey, *J. Nanobiotechnol.*, 2006, **4**, 9.
5 H. T. Huang, T. R. Ger, Y. H. Lin and Z. H. Wei, *Lab Chip*, 2013, **13**, 3098–3104.
6 A. Sharma, Y. C. Zhu, S. Thor, F. Zhou, B. Stadler and A. Hubel, *IEEE Trans. Magn.*, 2013, **49**, 453–456.
7 M. Safi, M. H. Yan, M. A. Guedeau-Boudeville, H. Conjeaud, V. Garnier-Thibaud, N. Boggetto, A. Baeza-Squiban, F. Niedergang, D. Averbeck and J. F. Berret, *ACS Nano*, 2011, **5**, 5354–5364.
8 F. Byrne, A. Prina-Mello, A. Whelan, B. M. Mohamed, A. Davies, Y. K. Gun'ko, J. M. D. Coey and Y. Volkov, *J. Magn. Magn. Mater.*, 2009, **321**, 1341–1345.
9 A. Hultgren, M. Tanase, C. S. Chen and D. H. Reich, *IEEE Trans. Magn.*, 2004, **40**, 2988–2990.
10 F. Johansson, M. Jonsson, K. Alm and M. Kanje, *Exp. Cell Res.*, 2010, **316**, 688–694.
11 A. Hultgren, M. Tanase, E. J. Felton, K. Bhadriraju, A. K. Salem, C. S. Chen and D. H. Reich, *Biotechnol. Prog.*, 2005, **21**, 509–515.
12 M. Tanase, E. J. Felton, D. S. Gray, A. Hultgren, C. S. Chen and D. H. Reich, *Lab Chip*, 2005, **5**, 598–605.
13 A. O. Fung, V. Kapadia, E. Pierstorff, D. Ho and Y. Chen, *J. Phys. Chem. C*, 2008, **112**, 15085–15088.
14 M. M. Song, W. J. Song, H. Bi, J. Wang, W. L. Wu, J. Sun and M. Yu, *Biomaterials*, 2010, **31**, 1509–1517.
15 X. H. Shi, A. von dem Bussche, R. H. Hurt, A. B. Kane and H. J. Gao, *Nat. Nanotechnol.*, 2011, **6**, 714–719.
16 Y. N. Xia, P. D. Yang, Y. G. Sun, Y. Y. Wu, B. Mayers, B. Gates, Y. D. Yin, F. Kim and Y. Q. Yan, *Adv. Mater.*, 2003, **15**, 353–389.
17 H. Schlorb, V. Haehnel, M. S. Khatri, A. Srivastav, A. Kumar, L. Schultz and S. Fahler, *Phys. Status Solidi B*, 2010, **247**, 2364–2379.
18 M. G. Maas, E. J. B. Rodijk, A. W. Maijenburg, D. H. A. Blank and J. E. ten Elshof, *J. Mater. Res.*, 2011, **26**, 2261–2267.
19 A. George, A. W. Maijenburg, M. G. Maas, D. H. A. Blank and J. E. ten Elshof, *ACS Appl. Mater. Interfaces*, 2011, **3**, 3666–3672.
20 A. W. Maijenburg, E. J. B. Rodijk, M. G. Maas, M. Enculescu, D. H. A. Blank and J. E. ten Elshof, *Small*, 2011, **7**, 2709–2713.
21 V. C. Sanchez, J. R. Pietruska, N. R. Miselis, R. H. Hurt and A. B. Kane, *Wiley Interdiscip. Rev.: Nanomed. Nanobiotechnol.*, 2009, **1**, 511–529.

22 L. A. Bauer, D. H. Reich and G. J. Meyer, *Langmuir*, 2003, **19**, 7043–7048.
23 P. H. Hoet, I. Bruske-Hohlfeld and O. V. Salata, *J. Nanobiotechnol.*, 2004, **2**, 12.
24 F. H. Nielsen, *Nutr. Today*, 1993, **28**, 14–19.
25 J. J. Pan, Q. S. Chang, X. Wang, Y. Son, Z. Zhang, G. Chen, J. Luo, Y. Y. Bi, F. Chen and X. L. Shi, *Chem. Res. Toxicol.*, 2010, **23**, 568–577.
26 J. Zhao, L. Bowman, X. Zhang, X. Shi, B. Jiang, V. Castranova and M. Ding, *J. Nanobiotechnol.*, 2009, **7**, 2.
27 M. Costa, *Fresenius' J. Anal. Chem.*, 1998, **361**, 381–385.
28 N. Gao, H. J. Wang and E. H. Yang, *Nanotechnology*, 2010, **21**, 105–107.
29 M. Z. Hossain and M. G. Kleve, *Int. J. Nanomed.*, 2011, **6**, 1475–1485.
30 D. Magnin, V. Callegari, S. Matefi-Tempfli, M. Matefi-Tempfli, K. Glinel, A. M. Jonas and S. Demoustier-Champagne, *Biomacromolecules*, 2008, **9**, 2517–2522.
31 N. S. Birenbaum, B. T. Lai, C. S. Chen, D. H. Reich and G. J. Meyer, *Langmuir*, 2003, **19**, 9580–9582.
32 I. T. Jeon, M. K. Cho, J. W. Cho, B. H. An, J. H. Wu, R. Kringel, D. S. Choi and Y. K. Kim, *J. Mater. Chem.*, 2011, **21**, 12089–12095.
33 G. Han, P. Ghosh and V. M. Rotello, *Nanomedicine*, 2007, **2**, 113–123.
34 R. Venkatesan, A. Pichaimani, K. Hari, P. K. Balasubramanian, J. Kulandaivel and K. Premkumar, *J. Mater. Chem. B*, 2013, **1**, 1010–1018.
35 P. Kohli, J. E. Wharton, O. Braide and C. R. Martin, *J. Nanosci. Nanotechnol.*, 2004, **4**, 605–610.
36 B. Das, K. Mandal, P. Sen and S. K. Bandopadhyay, *J. Appl. Phys.*, 2008, **103**, 013908-1-5.